

# An Empirical Calibration of Star Formation Rate Estimators

Daniel Rosa-González<sup>1</sup>, Elena Terlevich<sup>1\*</sup> and Roberto Terlevich,<sup>2†</sup>

<sup>1</sup> INAOE, Luis Enrique Erro 1, Tonantzintla, Puebla 72840, México.

<sup>2</sup> Institute of Astronomy, Madingley Road, CB3 OHA Cambridge, U.K.

Accepted . Received ; in original form 25 October 2018<sup>+</sup> SFR-v126

## ABSTRACT

The observational determination of the behaviour of the star formation rate (SFR) with look-back time or redshift has two main weaknesses: 1 - the large uncertainty of the dust/extinction corrections, and 2 - that systematic errors may be introduced by the fact that the SFR is estimated using different methods at different redshifts. Most frequently, the luminosity of the H $\alpha$  emission line, that of the forbidden line [OII] $\lambda 3727$  and that of the far ultraviolet continuum (UV) are used with low, intermediate and high redshift galaxies respectively.

To assess the possible systematic differences among the different SFR estimators and the role of dust, we have compared SFR estimates using H $\alpha$ , SFR(H $\alpha$ ), [OII] $\lambda 3727\text{\AA}$ , SFR(OII), UV, SFR(UV) and FIR, SFR(FIR) luminosities of a sample comprising the 31 nearby star forming galaxies having high quality photometric data in the UV, optical and FIR.

We review the different “standard” methods for the estimation of the SFR and find that while the standard method provides good agreement between SFR(H $\alpha$ ) and SFR(FIR), both SFR(OII) and SFR(UV) are systematically higher than SFR(FIR), irrespective of the extinction law.

We show that the excess in the SFR(OII) and SFR(UV) is mainly due to an overestimate of the extinction resulting from the effect of underlying stellar Balmer absorptions in the measured emission line fluxes. Taking this effect into consideration in the determination of the extinction brings the SFR(OII) and SFR(UV) in line with the SFR(FIR) and simultaneously reduces the internal scatter of the SFR estimations.

Based on these results we have derived “unbiased” SFR expressions for the SFR(UV), SFR(OII) and SFR(H $\alpha$ ). We have used these estimators to recompute the SFR history of the Universe using the results of published surveys. The main results are that the use of the unbiased SFR estimators brings into agreement the results of all surveys. Particularly important is the agreement achieved for the SFR derived from the FIR/mm and optical/UV surveys. The “unbiased” star formation history of the Universe shows a steep rise in the SFR from  $z = 0$  to  $z = 1$  with  $\text{SFR} \propto (1+z)^{4.5}$  followed by a decline for  $z > 2$  where  $\text{SFR} \propto (1+z)^{-1.5}$ . Galaxy formation models tend to have a much flatter slope from  $z = 0$  to  $z = 1$ .

**Key words:** Stars: formation, Galaxies: star forming, Galaxies: HII, Galaxies: evolution

## 1 INTRODUCTION

The knowledge of the history of star formation at cosmic scales is fundamental to the understanding of the formation and evolution of galaxies. Madau and collaborators

combined the results from the ultraviolet surveys of Lilly et al. (1996) with the information from the Hubble Deep Field to give an estimate of the star formation history from  $z = 0$  to  $z = 4$ . Subsequent studies have indicated the crucial role played by dust in the estimates of SFR. Large correction factors were suggested for  $z > 1-2$  by several authors (Meurer et al. 1997, Meurer, Heckman and Calzetti 1999, Steidel et al. 1999, Dickinson 1998). But even these

\* Visiting Fellow at IoA, UK

† Visiting Professor at INAOE, Mexico

large dust extinction corrections do not seem to be enough to bring the optical/UV SFR estimates in line with the mm/sub-mm ones (Hughes et al. 1998; Rowan-Robinson et al. 1997 (RR97); Chapman et al. 2001).

On top of the uncertainties associated with the extinction correction, most of the SFR estimates have been performed using expressions derived from spectra constructed using population synthesis methods, an approach that requires four rather uncertain ingredients: 1) an initial mass function (IMF); 2) a stellar evolutionary model grid giving the luminosity and effective temperature as a function of time; 3) a stellar atmospheres grid that assigns a spectrum to each star for a given luminosity and effective temperature, and 4) a star formation history. The fact that the redshift evolution of the SFR is constructed using different estimators at different redshift ranges is a potential source of systematic effects with redshift that can distort the shape of the evolutionary curve. In practice the  $H\alpha$  luminosity is used to estimate the SFR for galaxies with redshifts up to 0.4; the [OII]  $\lambda 3727\text{\AA}$  line, for those with  $0.4 > z > 1.0$  and the UV continuum luminosity for galaxies with  $z > 2.0$ . In addition, dust extinction corrections are not treated uniformly over the whole redshift range.

It is therefore important to ensure that there are no systematic differences between the different estimators and corrections that can distort the results.

This paper has two main aspects, in the first 5 sections we review the “standard” methods for the estimation of the SFR and test the consistency of the different SFR estimators by applying them to a sample of well studied nearby star forming galaxies and comparing the results. In the absence of systematic differences among them, all should give the same SFR for each one of the galaxies in the sample. We then use the results of the nearby sample to construct a set of “unbiased” SFR estimators and apply them to published surveys.

## 2 THE REFERENCE GALAXY SAMPLE

To critically test the possibility of systematic differences between the SFR estimators we have compiled from the literature a sample of all the nearby well studied star forming galaxies for which good data is available in  $H\alpha$ ,  $H\beta$ , [OII] $\lambda 3727$ , UV continuum and FIR. We call it the “reference” sample of galaxies.

The resulting sample consists of galaxies classified either as HII galaxy, Starburst (SB) or Blue Compact (BCG) and although it covers a range of galaxian properties, a large fraction of them is of low luminosity and low metal content. Work by Koo and collaborators (Koo et al. 1996, Lowenthal et al. 1997) has shown deep similarities between the faint blue galaxies found typically at  $z \sim 0.5$  and the type of galaxies in our sample. This could also be the case for Lyman limit galaxies (Giavalisco, Steidel & Macchetto 1996).

Spectroscopic data for 14 of the galaxies come from McQuade, Calzetti and Kinney (1995) where they combined spectral data in the UV from the IUE (Kinney et al. 1993) with optical observations. The optical spectra were obtained with the KPNO 0.9m telescope covering a spectral range from  $3500\text{\AA}$  to  $8000\text{\AA}$  with  $10\text{\AA}$  resolution. The circular aperture used by McQuade et al. (1995),  $13.5''$  in diameter, matches the  $10'' \times 20''$  IUE aperture. Therefore no area renormalization was necessary for these galaxies when comparing UV with optical data.

Optical data for other 12 galaxies were obtained by Storchi-Bergmann, Kinney and Challis (1995) and combined with the (Kinney et al. 1993) IUE ultraviolet atlas. The optical observations were made with the 1m and 1.5m CTIO telescopes. They used a long slit of 10 arcsecond width which was vignetted to equal the  $10'' \times 20''$  IUE aperture. The 1m telescope covered a range from  $3200$  to  $6400\text{\AA}$  with a resolution of  $5.5\text{\AA}$  and the 1.5m telescope covered from  $6400$  to  $10000\text{\AA}$  with a resolution of  $8\text{\AA}$ . In general their spectra flux levels agree within 20% with the spectra from the IUE satellite. In the cases where the differences were larger (observations made under non-photometric conditions) they assumed that the flux given by the IUE observations is the correct one.

The optical spectra of CAM0840, TOL1247 and CAM1543 were observed by Terlevich et al. (1991). TOL1247 was observed under photometric conditions with the 3.6m ESO telescope and an  $8 \times 8$  arcsec aperture. The spectra of CAM0840 and CAM1543 were obtained at Las Campanas Observatory with the 2.5m telescope. An aperture of  $2 \times 4$  arcsec and a resolution of about  $5\text{\AA}$  were used. The ultraviolet spectra of these galaxies are from IUE satellite observations, Terlevich et al. (1993) (CAM0840 and TOL1247) and Meier & Terlevich (1981) (CAM1543).

The optical data of MRK309 is from the UCM objective-prism survey (Gallego et al. 1996). The UV data comes from the observations made with IUE and reported by McQuade et al. (1995).

Table 1 shows the complete sample of star forming galaxies used in this study. All the objects are located at large galactic latitudes ( $|b| > 25$ ). The apparent blue magnitudes are from De Vaucouleurs et al. (1991) and are corrected for galactic extinction, internal extinction and aperture differences. Radial velocities were corrected by the Local Group motion using the NED<sup>†</sup> velocity correction software (Table 1).

The  $60\text{\mu m}$  IRAS data for all the galaxies come from Moshir et al. (1990).

We computed the equivalent width of  $H\beta$  using the easily deduced expression,

$$EW(H\beta) = \frac{L(H\beta)}{L_c(4861\text{\AA})} = 2.5 \times 10^{-32} \frac{L(H\beta)}{\text{erg s}^{-1}} 10^{(0.4M_B)} \quad (1)$$

where  $L(H\beta)$  and  $L_c(4861\text{\AA})$  are the  $H\beta$  and adjacent continuum luminosities respectively. The field of view used to estimate  $M_B$  is larger than the apertures for the spectroscopic observations, therefore the estimated  $EW(H\beta)$  represents a lower limit. Where  $M_B$  was not available, as for CAM0840, CAM1543 and TOL1247, we used  $EW(H\beta)$  from the spectrophotometry of Terlevich et al. (1991).

The extinction correction to the observed fluxes both on the continuum and on the emission lines was estimated following standard procedures. Two different extinction curves were used: the Milky Way extinction law (MW) given by

<sup>†</sup> NASA/IPAC Extragalactic Database

Name	Type	$m_B$	Velocity ( km s $^{-1}$ )	F(H $\alpha$ )	F(H $\beta$ )	F(H $\gamma$ )	F(OII)	F $_{\lambda}$ (UV) (*)	F $_{\nu}$ (60 $\mu$ m)	Ref.
NGC7673	HII	12.86	3673.20	608.0	109.8	22.1	446.6	14.6	4.95	(a)
CAM0840	HII	—	9000.00	127.1	37.1	15.8	46.1	3.6	0.29	(b)
CAM1543	HII	—	11392.11	191.0	52.5	22.6	31.3	4.1	—	(e)
TOL1247	HII	—	14400.00	504.5	134.9	58.7	159.2	11.0	0.51	(b)
NGC1313	HII	9.29	269.86	148.4	17.3	3.5	105.4	6.60	14.56	(d)
NGC1800	HII	12.87	614.07	125.9	26.0	4.0	199.3	15.00	0.77	(d)
ESO572	HII	14.16	871.51	647.9	106.7	52.8	283.7	19.95	0.86	(d)
NGC7793	HII	9.37	253.35	221.9	33.0	—	110.6	9.37	8.89	(d)
UGCA410	BCDG	15.45	854.20	324.4	80.2	21.5	104.6	10.4	0.30	(a)
UGC9560	BCDG	14.81	1305.00	529.4	144.6	50.7	334.5	18.4	0.71	(a)
NGC1510	BCDG	13.45	737.95	512.1	116.8	31.6	340.9	16.52	0.89	(d)
NGC1705	BCDG	12.58	401.23	434.1	130.0	22.3	265.0	93.67	0.87	(d)
NGC4194	BCG	12.86	2598.46	1946.6	239.1	70.1	385.3	14.2	23.52	(a)
IC1586	BCG	14.74	6045.25	229.3	38.8	8.6	138.8	5.0	0.96	(a)
MRK66	BCG	15.00	6656.66	121.3	43.2	11.0	148.2	9.9	0.54	(a)
Haro15	BCG	—	6498.24	301.1	81.0	25.7	264.6	18.15	1.35	(d)
NGC1140	BCG	12.56	1503.13	1400.0	350.3	121.3	1010.0	44.15	3.36	(d)
NGC5253	BCG	10.87	270.61	7717.0	2406.0	973.2	4370.3	99.05	30.51	(d)
MRK542	BCG	15.80	7518.56	88.9	17.1	—	3.8	5.75	0.48	(a)
NGC6217	SB	11.66	1599.81	607.4	92.9	14.8	108.1	15.3	11.05	(a)
NGC7714	SB	12.62	2993.82	2795.8	539.9	196.9	951.1	26.5	10.44	(a)
NGC1614	SB	13.28	4688.15	1069.4	92.0	19.8	95.2	4.8	32.71	(a)
NGC6052	SB	13.40	4818.45	565.0	122.7	39.6	376.2	9.9	6.31	(a)
NGC5860	SB	14.21	5532.07	296.7	26.8	—	15.4	5.5	1.64	(a)
NGC6090	SB	14.51	8986.89	675.3	123.7	42.0	153.6	9.6	6.45	(a)
IC214	SB	14.16	9161.10	152.2	21.4	5.4	35.9	6.2	5.22	(a)
MRK309	SB	14.61	12918.07	108.0	16.2	—	4.4	2.4	3.43	(c)
NGC3049	SB	12.77	1321.32	513.1	116.1	51.9	148.5	10.25	2.82	(d)
NGC4385	SB	12.90	1981.44	950.0	150.7	51.2	261.0	11.82	4.73	(d)
NGC5236	SB	7.98	304.31	4507.0	940.1	154.7	440.0	185.47	110.30	(d)
NGC7552	SB	11.13	1571.17	2064.0	277.8	44.5	243.8	19.97	72.03	(d)

**Table 1.** Observed properties of the galaxy sample. The blue apparent magnitudes are from De Vaucouleurs et al. (1991). The emission lines and the ultraviolet continuum fluxes are from (a) McQuade et al. (1995), (b) Terlevich et al. (1993), (c) Gallego et al. (1996) and McQuade et al. (1995), (d) Storchi-Bergmann et al. (1995), (e) Meier & Terlevich (1981) and Terlevich et al. (1991). Units for the intensities are  $10^{-15}$  erg s $^{-1}$  cm $^{-2}$  except (\*) where the units are  $10^{-15}$  erg s $^{-1}$  cm $^{-2}$  Å $^{-1}$ . The FIR fluxes are IRAS at 60  $\mu$ m in Janskys.

Seaton (1979) and Howarth (1983) and the Large Magellanic Cloud one (LMC) given by Howarth (1983). A detailed description of the procedure can be found in Appendix 1.

### 3 STANDARD SFR ESTIMATES

In this section we describe the four estimators we have used to compute the SFR from the luminosities of the H $\alpha$  and [OII] $\lambda$ 3727 nebular lines, the UV luminosity and the FIR continuum. The expressions used here are the ones we found most frequently referred to in the literature. All expressions are for a Salpeter IMF ( $N(m) \propto m^{-2.35}$ ) with masses varying from 0.1 to 100  $M_{\odot}$ , solar metallicity and continuous star formation. To convert the fluxes into luminosities we used a Hubble constant of 70 km s $^{-1}$  Mpc $^{-1}$ .

#### 3.1 From H $\alpha$ Luminosities.

For the estimate of the SFR from H $\alpha$  luminosities we used the expression given by Kennicutt, Tamblyn and Congdon (1994),

$$SFR(H\alpha)(M_{\odot}yr^{-1}) = 7.9 \times 10^{-42} L_{H\alpha}(\text{erg s}^{-1}) \quad (2)$$

valid for a  $T_e=10^4$ K and Case B recombination, i.e. all the ionizing photons are processed by the gas.

#### 3.2 From [OII] $\lambda$ 3727 Luminosities.

The doublet [OII] $\lambda$ 3727 luminosity is used as a SFR tracer for objects with redshift larger than 0.4 where H $\alpha$  is shifted outside the optical range. Unlike H $\alpha$ , the [OII] $\lambda$ 3727 intensity depends not only on the electron temperature and density but also on the degree of ionization and on the metallicity of the gas. In practice a semi-empirical approach is used combining the SFR(H $\alpha$ ) with the average H $\alpha$  / [OII] $\lambda$ 3727 ratio given by Gallagher et al. (1989) using a sample of 75 blue galaxies and by Kennicutt (1992) from a sample of 90 normal and irregular galaxies.

$$SFR([\text{OII}])(M_{\odot}yr^{-1}) = 1.4 \times 10^{-41} L_{OII}(\text{erg s}^{-1}) \quad (3)$$

### 3.3 From UV Continuum Luminosities.

The UV continuum luminosity is used as a SFR tracer in objects with redshift higher than 1–2. At these redshifts all strong emission lines, apart from Ly $\alpha$ , are shifted outside the optical range.

In young stellar clusters, the UV spectrum is dominated by the continuum emission of massive stars. In evolutionary synthesis models of starbursts, after a short initial transient phase, the UV luminosity per unit frequency becomes proportional to the SFR,

$$SFR(UV)(M_{\odot} \text{yr}^{-1}) = 1.4 \times 10^{-28} L_{\nu}(\text{erg s}^{-1} \text{Hz}^{-1}) \quad (4)$$

This equation is valid from 1500 to 2800 Å where the integrated spectrum is nearly flat in  $F_{\nu}$  for a Salpeter IMF, continuous mode of star formation and solar metallicity. This region of the UV is not affected by the Ly $\alpha$  forest and the contribution from old populations is still very small (Kennicutt 1998, Madau et al. 1998).

This SFR indicator though, is extremely sensitive to uncertainties in the reddening correction.

### 3.4 From FIR.

To transform the observed 60 $\mu\text{m}$  luminosity to SFR we assumed that a fraction  $\epsilon$  of the ultraviolet/optical flux emitted by stars is absorbed by dust and reemitted as thermal emission in the far infrared (10 – 300  $\mu\text{m}$ ). Work by, among others, Mas-Hesse and Kunth (1991) indicate that even for a small amount of reddening the fraction  $\epsilon$  is very close to unity. This, plus the fact that no dust extinction correction is necessary, justifies the assumption that the FIR luminosity is an excellent indicator of the total UV/optical emissivity of a galaxy. Thus, the relation between the total FIR luminosity and the star formation rate (Kennicutt 1998) is

$$SFR(\text{FIR})(M_{\odot} \text{yr}^{-1}) = 1/\epsilon \ 4.5 \times 10^{-44} L_{\text{FIR}}(\text{erg s}^{-1}) \quad (5)$$

where the FIR luminosity is given by  $L_{\text{FIR}} \sim 1.7 \times L_{60\mu\text{m}}$  (Chapman et al. 2000).

A difficult parameter to quantify is the fraction of ionizing photons that escape from the nebula. Heckman et al (2001) show that in five of the UV brightest local starburst galaxies the fraction of photons escaping is less than about 6% while Steidel, Pettini and Adelberger (2001) claim a higher escape fraction. Bearing in mind that the two samples differ, these results may not be contradictory. Tenorio-Tagle et al. (1999) have shown that the escape of photons from a starburst may be time dependent with a very large escape probability during the most luminous phases and little escape at other stages.

It is important to point out that if the dust and ionized gas distributions are similar, i.e. they coexist spatially, the FIR and the emission line luminosities will be similarly affected by the escape of photons. Thus, under this condition, the ratios of emission line fluxes to FIR flux are, to first order, independent of the fraction of escaped photons and therefore not very sensitive to variations in the photon escape from nebula to nebula.

## 4 COMPARING THE DIFFERENT SFR ESTIMATORS

We have applied the commonly used SFR estimators to our reference sample of star forming galaxies. Given that the estimators are all for the same IMF and stellar models we do not expect these aspects to introduce any scatter. Figure 1 shows the SFR(H $\alpha$ ), SFR(OII) and SFR(UV) plotted against the SFR(FIR). Clearly the sample shows a correlation plus a large scatter.

To simplify the analysis and simultaneously make use of the fact that SFR(FIR) is probably the best SFR estimator available, we will use in what follows FIR normalized SFR, i.e. the SFR relative to SFR(FIR). The FIR normalized SFR(H $\alpha$ ), SFR(OII) and SFR(UV) are:

$$\begin{aligned} \Delta H\alpha &= \log \frac{SFR(H\alpha)}{SFR(\text{FIR})} \\ \Delta OII &= \log \frac{SFR(OII)}{SFR(\text{FIR})} \\ \Delta UV &= \log \frac{SFR(UV)}{SFR(\text{FIR})} \end{aligned}$$

This is better seen in the distribution histograms of the normalized SFR as shown in Figure 2. As reference we included in parts a,d,g of the figure the normalized SFR computed using the observed luminosities. The central and right columns show the dust extinction corrected ratios using the MW and the Calzetti extinction laws respectively. The corrections were applied following the common methodology and are described in Appendix A.

Our main conclusion is that irrespective of the extinction law applied, the SFR(H $\alpha$ ) is close to the SFR(FIR) while both SFR(OII) and SFR(UV) show a clear excess. The excess is much larger for SFR(UV) than for SFR(OII) suggesting a wavelength dependent effect, probably an extinction over-correction. Bearing in mind that our reference sample has a large fraction of low metallicity and low extinction galaxies this result suggests that applying these standard methods to estimate SFR will systematically overestimate the SFR in samples at intermediate and high redshifts where either SFR(OII) or SFR(UV) are used. This result is in apparent contradiction with what has been found and shown in Madau-type plots in recent years, where the SFR obtained from UV and optical data are much lower than that obtained from mm and sub-mm observations at intermediate and high redshifts. In order to reach agreement between both determinations, fixed (and somehow arbitrary) amounts of extinction have been applied to the UV/optical data, because at the moment, the intermediate and high redshift samples do not allow a reliable determination of the dust extinction. It is worth noting that Steidel et al. (1999) applied a fixed correction to their sample that is close to the average  $\Delta UV$ . On a positive note we should indicate that the application of the reddening corrections reduce considerably the scatter in all three normalized SFR estimators as we will show below.

It is important to clarify the origin of the detected excess in the extinction corrected  $\Delta OII$  and  $\Delta UV$ . There is one effect that is not normally taken into account, namely that the presence of an underlying young stellar population with deep Balmer absorptions will bias the observed emission line ratios towards larger Balmer decrement values, mimicking

the dust extinction effect. In the next section we will recalculate the SFR for the different tracers but including an estimation of the effect of an underlying population. We will also estimate the effect of photon escape in  $\Delta$ UV.

## 5 UNDERLYING POPULATION AND PHOTON ESCAPE

### 5.1 Underlying absorption corrections to the emission line fluxes

A clear signature of a population of young and intermediate age stars is the presence of the Balmer series in absorption in their optical spectrum. A complication is that in star forming objects, the Balmer emission lines from the ionized gas appear superimposed to the stellar absorption lines. This effect, growing in importance towards the higher order Balmer lines, is illustrated in Figure 3 where an example (NGC 1510) is shown. It can be seen that, while  $H\beta$  emission is moderately affected by the absorption, all of the  $H\delta$  emission is lost into the absorption. The equivalent width of the Balmer absorptions peaks at  $H\delta - H\epsilon$  and there is no detection of any absorption in  $H\alpha$ . This is due to the facts that the  $H\alpha$  absorption equivalent width is much smaller than that of  $H\beta$ , and that the wings of the  $H\alpha$  absorption are difficult to detect due to the presence of forbidden [NII] doublet emission at  $\lambda 6548\text{\AA}$  and  $\lambda 6584\text{\AA}$ , right on top of both wings. In spectra of poorer S/N or lower spectral resolution than that of Figure 3, the wings of the Balmer absorptions are not detected and the result is an underestimate of the emitted fluxes and, more important for luminosity determinations, an overestimate of the internal extinction (Olofsson 1995).

The observed ratio between two emission lines (e.g.  $H\alpha$  and  $H\beta$ ), when the underlying absorption is included, is:

$$\frac{F(H\alpha)}{F(H\beta)} = \frac{F_+(H\alpha) - F_-(H\alpha)}{F_+(H\beta) - F_-(H\beta)} \quad (6)$$

where  $F_+(H\alpha)$  and  $F_+(H\beta)$  are the intrinsic emission line fluxes and  $F_-(H\alpha)$  and  $F_-(H\beta)$  are the intrinsic fluxes of the corresponding absorption lines. This expression is correct in the case that the emission and the absorption lines have approximately equal widths.

Including the relation between the equivalent width, the flux of the continuum and the intensity of the line in equation 6 we obtain,

$$\frac{F(H\alpha)}{F(H\beta)} = \frac{2.86 - PQ \frac{F_C(H\alpha)}{F_C(H\beta)}}{1 - Q} = \frac{2.86 \left[ 1 - PQ \frac{EW_+(H\beta)}{EW_+(H\alpha)} \right]}{1 - Q} \quad (7)$$

where,  $F_C(H\alpha)$  and  $F_C(H\beta)$  are the continuum in  $H\alpha$  and  $H\beta$  respectively,  $EW_+$  and  $EW_-$  are the equivalent widths in emission and in absorption respectively for the different lines,  $Q = \frac{EW_-(H\beta)}{EW_+(H\beta)}$  is the ratio between the equivalent widths of  $H\beta$  in absorption and in emission,  $P = \frac{EW_-(H\alpha)}{EW_-(H\beta)}$  is the ratio between the equivalent widths in absorption of  $H\alpha$  and  $H\beta$  and  $F_+(H\alpha)/F_+(H\beta) = 2.86$  is the theoretical ratio between  $H\alpha$  and  $H\beta$  in emission for Case B recombination (Osterbrock 1989).

The value of  $P$  can be obtained from spectral evolutionary calculations like those of Olofsson (1995). For the case

of solar abundance and stellar masses varying between 0.1 and 100  $M_\odot$  within a Salpeter IMF, the value of  $P$  changes between 0.7 and 1 for ages between 1 and 15 million years respectively. This variation in the  $P$  parameter produces a change in the estimated  $F(H\alpha)/F(H\beta)$  ratio of less than 2%, so in what follows we assume  $P=1$ .

For an instantaneous burst, the ratio  $\frac{EW_+(H\beta)}{EW_+(H\alpha)}$  varies between 0.14 and 0.26 (Mayya (1995), Leitherer & Heckman (1995)).

The corresponding equation for  $H\gamma$  and  $H\beta$  is:

$$\frac{F(H\gamma)}{F(H\beta)} = \frac{0.47 - GQ}{1 - Q} \quad (8)$$

where  $G = \frac{EW_-(H\gamma)}{EW_-(H\beta)}$  is the ratio between the equivalent widths in absorption of  $H\gamma$  and  $H\beta$  and we assume for the respective emissions an intrinsic ratio of 0.47 for Case B recombination (Osterbrock 1989).

The evolution of the equivalent width of the Balmer absorption lines has been analyzed by González Delgado, Leitherer and Heckman (1999). In their models the parameter  $G$  is almost constant in time and independent of the adopted star formation history. We fixed the value of  $G$  to 1 as suggested by their results.

The effect of the underlying stellar absorptions is shown as a vector  $Q$  in Figure 4 (from equations 7 and 8). The whole time dependence is shown by the three closely grouped vectors. Its range is much smaller than typical observational errors. Dust extinction is also represented by a vector in the same plane (equation A8). It is possible, as these two vectors are not parallel, to solve simultaneously for underlying absorption ( $Q$ ) and extinction ( $Av$ ) for every object for which  $F(H\gamma)$ ,  $F(H\beta)$  and  $F(H\alpha)$  are measured.

We further illustrate the presence of underlying Balmer absorption in star forming galaxies in Figure 5 where we have plotted the galaxies from our sample in the  $\log(F(H\gamma)/F(H\beta))$  vs.  $\log(F(H\alpha)/F(H\beta))$  plane. Also shown are the vectors depicting dust extinction and the underlying absorption. Clearly, most observational points occupy the region below the reddening vector and to the right of the Balmer absorption vector. In the absence of underlying absorption all points should be distributed along the extinction vector. The fact that there is a clear spread below the extinction vector gives support to the underlying absorption scenario. We also find that the objects with smaller equivalent width of  $H\beta$  are systematically further away from the pure extinction vector.

Four galaxies (NGC 3049, ESO 572, MRK 66 and NGC 1705) fall outside the space defined by the extinction and underlying absorption vectors, although two of them are within the errors. The other two (ESO 572 and MRK 66) are faint and reported as having been observed in less than optimum conditions in the original observations paper.

We have used this method to estimate simultaneously the “real” visual extinction  $Av^*$  and the underlying Balmer absorption  $Q$ <sup>§</sup>. The values of  $Av^*$  were then applied to the UV continuum and the emission line fluxes; the corrected values are listed in Table 2.

<sup>§</sup> See Appendix A for a detailed discussion on the dust extinction corrections to the observed fluxes.

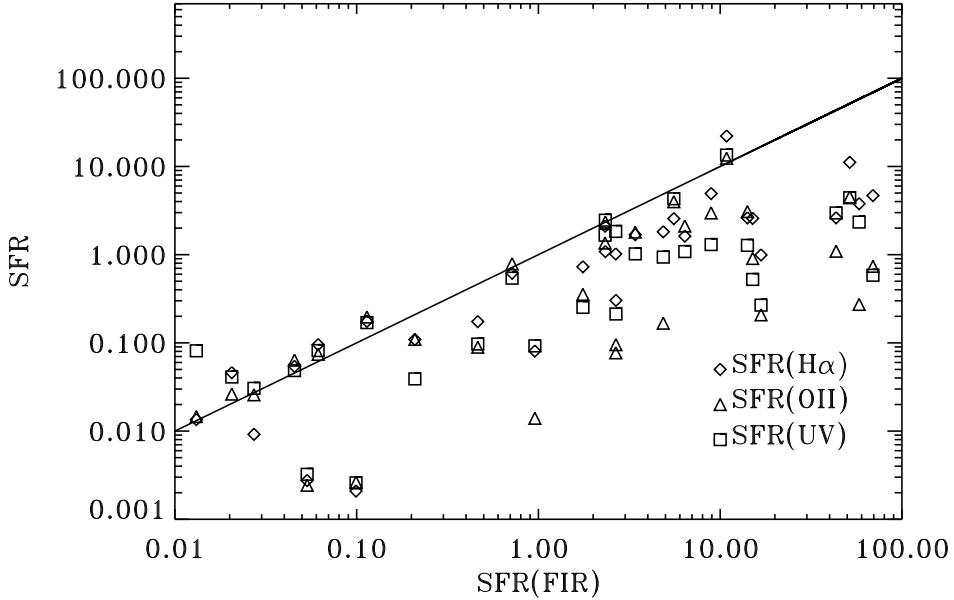


**Figure 1.** Standard SFR estimators vs. SFR(FIR). No extinction corrections were applied to the data. The solid line represents equal values.

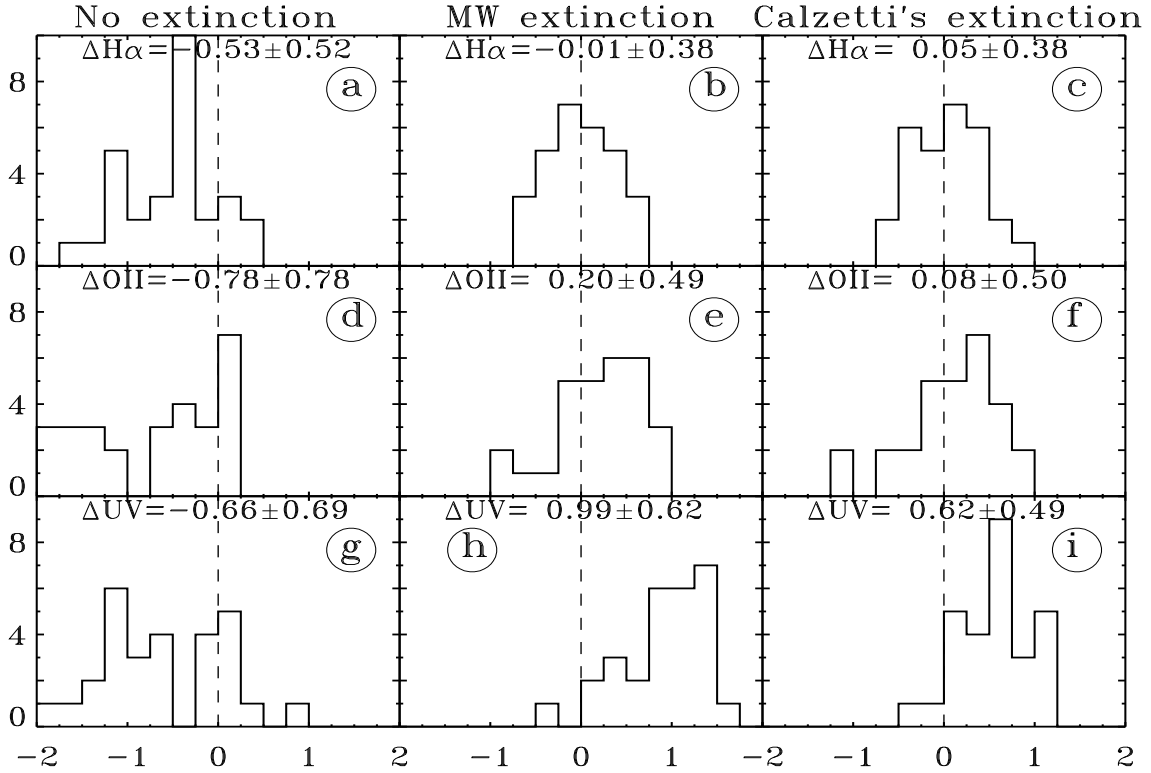


**Figure 2.** Histograms of the SFR rates given by the different tracers normalized to the SFR(FIR). In the left panels (a,d,g) no corrections were applied to the data. In the central panels (b,e,h) we corrected the  $\text{H}\alpha$ ,  $[\text{OII}]\lambda 3727$  and UV continuum by using the MW extinction curve. In the right panels (c,f,i) the  $\text{H}\alpha$ ,  $[\text{OII}]\lambda 3727$  and UV continuum were corrected with Calzetti's extinction law. The median and standard deviation are given for each case. The number of objects is 29.

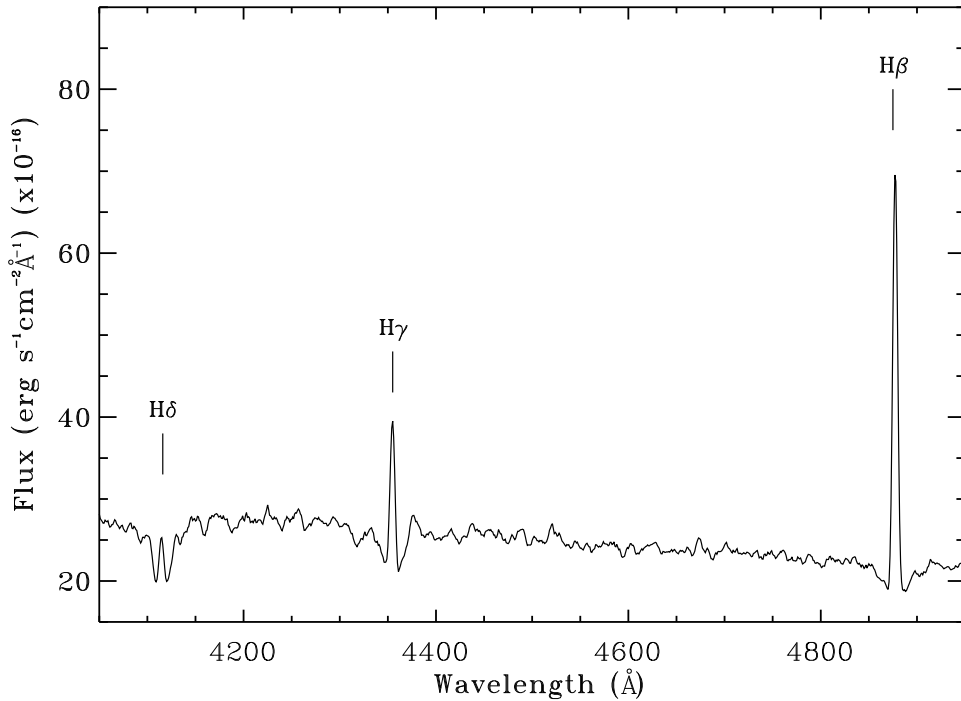


**Figure 3.** A blue spectrum of the star forming galaxy NGC 1510 is shown to illustrate the effect of stellar Balmer absorptions in the measurement of the emission line strengths.

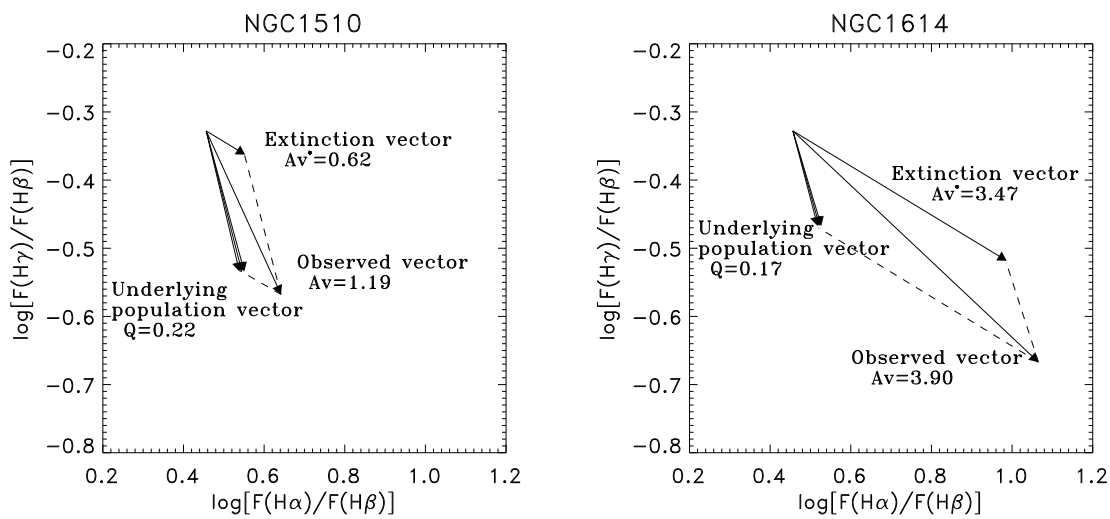


**Figure 4.** Logarithmic ratio of  $F(H\alpha)/F(H\beta)$  vs.  $F(H\gamma)/F(H\beta)$ . The “observed vector” (from the intrinsic values given by recombination theory to the observed ratio) can be decomposed in two vectors, one is due to pure extinction and is given by Equation A8, the other one is given by Equations 7 and 8 and shows the effect of an underlying stellar population which is characterized by  $Q$  (see text). Plotted are the cases for NGC 1614 and NGC 1510. NGC 1614 is an example where the underlying absorption correction to the extinction estimate is not very large. NGC 1510 on the other hand, has a large correction.

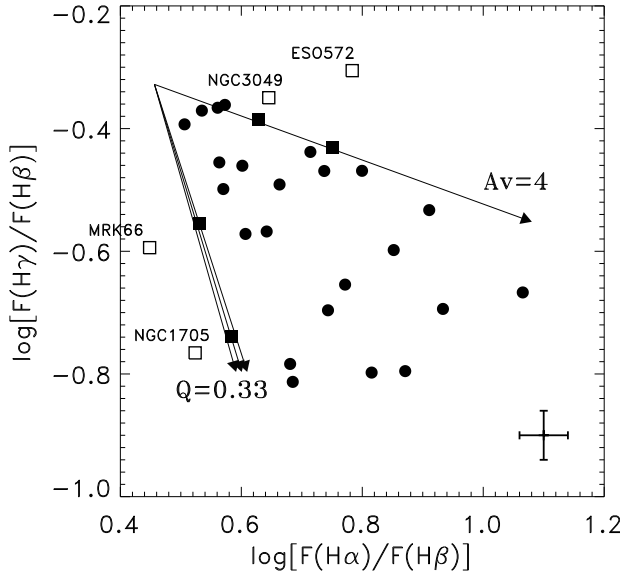


**Figure 5.** The galaxies from our sample are plotted in the Balmer decrement plane  $\log(F(H\alpha)/F(H\beta))$  vs.  $\log(F(H\gamma)/F(H\beta))$ . The vectors indicate the direction of shifts due to extinction or underlying absorption from the intrinsic values given by recombination. The cross indicates typical  $1\sigma$  errors in the line ratios. Most points are, within the errors, below the reddening line and to the right of the underlying Balmer absorption line.

Figure 6 shows the result of taking into account the corrections for Balmer absorptions due to an underlying stellar population. The medians of both  $\Delta OII$  and  $\Delta H\alpha$  are close to zero indicating that including the underlying absorption correction brings into agreement the SFR in the optical with those in the FIR. At the same time  $\Delta UV$  shows still a positive value indicating an excess with respect to the FIR estimate. We must remember that while the ratio of emission line fluxes to FIR flux is not very sensitive to changes in the photon escape from object to object, this is not the case for the ratio of UV continuum to FIR fluxes. The reason being that while in the UV continuum we are detecting directly the escaped photons, i.e. those that do not heat the dust or ionize the gas, the emission lines and FIR fluxes are reprocessed radiation, i.e. the product of the radiation that does not escape the region.

A striking aspect is the large reduction in the r.m.s. scatter in the  $\Delta UV$  from 0.70 before corrections to 0.39 after corrections, i.e. about half the original value. This simple fact suggests the goodness of the corrections applied to the data. This aspect is also illustrated in Figure 7 when compared to Figure 1.

## 5.2 Photon Escape

As discussed above, while  $\Delta OII$  and  $\Delta H\alpha$  are not very sensitive to the fraction of escaped photons,  $\Delta UV$  is. The escape of UV photons can be quantified by the parameter  $\epsilon$  (Rowan-Robinson & Efstathiou 1993) by assuming that

$$\begin{aligned} L_{FIR} &= \epsilon F_{Bol} \\ L_{UV} &= (1 - \epsilon) F_{Bol} \end{aligned} \quad (9)$$

where  $(1 - \epsilon)$  represents the escaped fraction.

Thus, the reprocessed fraction  $\epsilon$  can be estimated through the observed  $60\mu m$  and ultraviolet luminosities as

$$\epsilon = \frac{1}{1 + \frac{L_{UV}}{L_{60\mu m}}} \quad (10)$$

where the luminosities are given by

$$\begin{aligned} L_{UV}(erg\ s^{-1}) &= F_\lambda(UV) \times 2000\text{\AA} \\ L_{60\mu m}(erg\ s^{-1}) &= F_\nu(60\mu m) \ 5 \ 10^{12} Hz \ 10^{-23} \end{aligned} \quad (11)$$

The values of the UV flux in units of  $erg\ s^{-1}cm^{-2}\text{\AA}^{-1}$  and the fluxes at  $60\mu m$  in Jy are given in Table 1 and the calculated values of the escape fraction  $1 - \epsilon$ , in Table 2.

The results of including the photon escape are also shown in the  $\Delta UV$  histograms of Figure 8. As discussed above, under the simple assumption that dust and ionized gas have the same spatial distribution, the values of  $\Delta H\alpha$  and  $\Delta OII$  do not change with respect to Figure 6.

In the left panel, the UV continuum was corrected using Steidel et al. (1999) simple approach of multiplying the observed UV flux by a fixed amount ( $\times 5$ ) which corresponds to the average correction found in a sample of local starburst galaxies (Calzetti et al. 1994). The fact that the average correction for Calzetti's sample and the average correction for our sample are almost identical suggests that both samples have been drawn from the same family of objects, i.e. they are similar samples.

The central panel shows the result of using the MW extinction law and applying to the observed values the expression A5 where the visual extinction is  $Av^*$ . The panel at the right shows the result of using the extinction law given by Calzetti et al. (1994). Also in this case the visual extinction is  $Av^*$ .

Inspection of the  $\Delta UV$  distribution in figures 2, 6 and 8 shows that at least for the galaxies in the "reference" sample, the escape of photons is a minor effect compared to the underlying Balmer absorption.

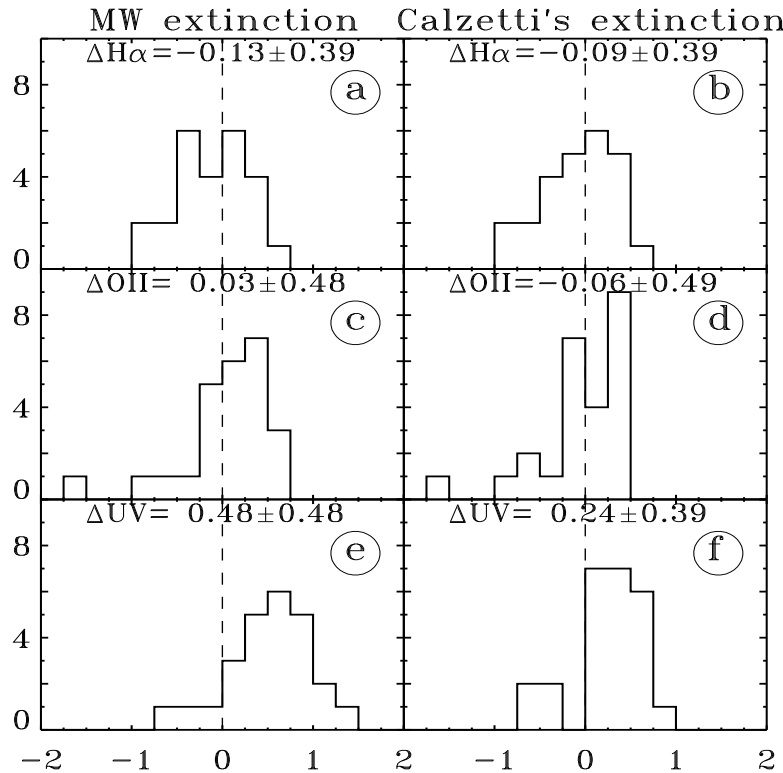


**Figure 6.** The figure shows the histograms of the normalized SFR after the underlying stellar absorption effect is deducted from the extinction estimates, i.e.  $A_V^*$  is used instead of  $A_V$  (Section 5.1). Panels a, c, e show the distributions after correcting the H $\alpha$ , [OII] $\lambda 3727$  and UV continuum using the MW extinction curve. b, d, and f show the result of using Calzetti's extinction curve. The median and standard deviation are given for each case. The total number of objects is 25.

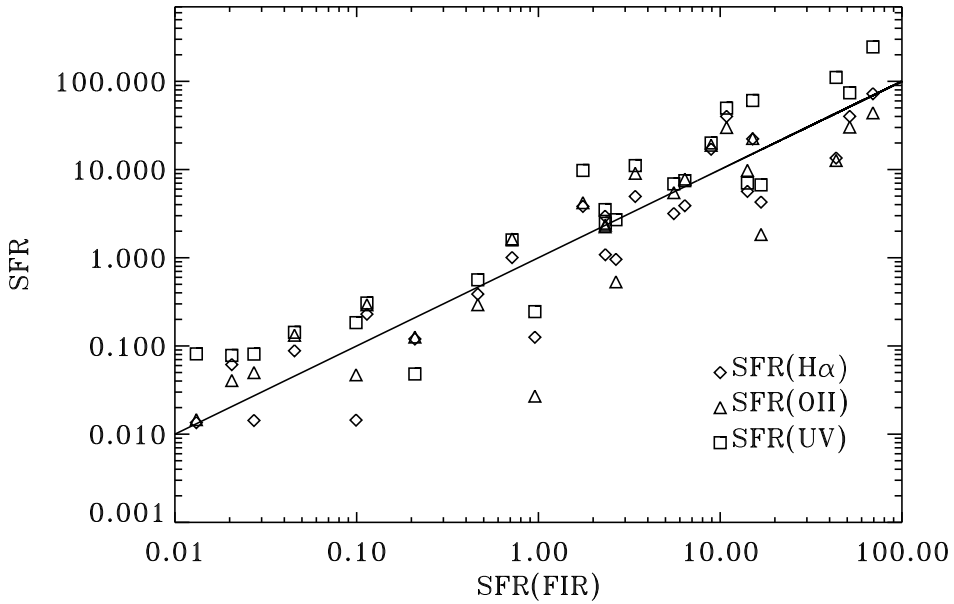


**Figure 7.** Corrected SFR estimators vs. SFR(FIR). The corrections include the underlying Balmer absorption (see Section 5.1) and photon escape (see Section 5.2). The solid line represents equal values.

Comparing the MW and Calzetti's extinction corrections we can conclude that the corrections using the Calzetti's extinction curve give a SFR(UV) identical inside the errors to the SFR(FIR) plus a substantial reduction in the dispersion of the SFR estimates. These two points jus-

tify the use of Calzetti's extinction corrections in samples of starburst galaxies similar to the ones used in this work. It is a remarkable result that the application of our method succeeds in cutting down the scatter present in the original data to less than a half. These two results, i.e. the very

Name	Av	Av*	$Q \times 100$	$\beta$	$(1 - \epsilon)$	EW(H $\beta$ )
NGC7673	1.84	1.11	27	-1.50	0.11	4.69
CAM0840	0.50	0.43	3	-1.26†	0.33	121★
CAM1543	0.67	0.67	0	-0.70†	—	224★
TOL1247	0.75	0.75	0	-0.47†	0.46	97★
NGC1313	3.06	2.45	23	-0.60‡	0.02	0.03
NGC1800	1.47	0.56	33	-1.65	0.56	1.10
ESO572	2.10	1.87	0	-1.96†	0.48	14.81
NGC7793	2.38	—	—	-1.34	0.04	0.06
UGCA410	0.97	0.37	23	-1.84	0.58	36.52
UGC9560	0.69	0.34	14	-2.02	0.51	36.63
NGC1510	1.19	0.62	22	-1.71	0.43	8.42
NGC1705	0.43	0.0	31	-2.42	0.81	4.20
NGC4194	2.91	2.73	8	-0.26	0.02	10.14
IC1586	2.02	1.37	25	-0.91	0.17	9.51
MRK66	0.00	0.00	23	-1.94	0.42	13.50
Haro15	0.73	0.27	18	-1.48	0.35	—
NGC1140	0.93	0.62	13	-1.78	0.34	11.19
NGC5253	0.32	0.12	9	-1.33	0.11	16.07
MRK542	1.66	—	—	-1.32	0.32	11.23
NGC6217	2.30	1.46	31	-0.74	0.05	1.30
NGC7714	1.65	1.57	4	-1.23	0.09	18.40
NGC1614	3.90	3.47	17	-0.76	0.01	5.82
NGC6052	1.33	0.98	14	-0.72	0.06	8.68
NGC5860	3.77	—	—	-0.91	0.12	4.02
NGC6090	1.80	1.62	8	-0.78‡	0.06	25.00
IC214	2.54	2.08	18	-0.61	0.05	3.14
MRK309	2.36	—	—	2.08†	0.03	3.68
NGC3049	1.21	1.01	0	-1.14	0.13	4.49
NGC4385	2.20	2.10	4	-1.02	0.09	6.60
NGC5236	1.44	0.56	32	-0.83	0.06	0.44
NGC7552	2.66	1.85	30	0.48	0.01	2.38

**Table 2.** Extinction properties, ultraviolet slope and photon escape probability of the galaxy sample. The second column is the extinction in magnitudes obtained with the MW extinction curve (see Appendix) without taking into account the effect of the underlying population. The third column is the extinction in magnitudes obtained by combining the MW extinction curve with the effect of an underlying population. The ratio between the equivalent widths of H $\beta$  in absorption and in emission as defined in Section 5.1 is given in the fourth column. Values of the ultraviolet slope  $\beta$  (see appendix) are from Meurer et al. (1999) except for those marked with a ‡ where the values were extracted from Calzetti et al. (1994) and those marked with a † where we calculated ourselves the parameter  $\beta$  from the IUE data base spectra, following Calzetti et al. (1994) prescription. The escape probability  $\epsilon$  is given in the sixth column (see text). Equivalent widths were calculated using Equation 1 except when marked with a ★ where they were taken from published spectroscopy.

close agreement between the SFR(UV) and SFR(FIR) plus the rather small scatter in the ratio of these two estimators gives confidence in the use of our approach to estimate dust extinction and star formation rates in starburst galaxies.

## 6 UNBIASED SFR ESTIMATORS

The central result we have found is that the extinction correction including the effects of an underlying stellar Balmer absorption brings into agreement all four SFR estimators, and that the photon escape correction seems to play a minor role.

We have seen that the SFR given by the UV continuum is equal to the SFR given by the FIR if the extinction correction is estimated using the Calzetti extinction curve and including the underlying Balmer absorption corrections. It is reassuring that the simple inclusion of the underlying absorption correction brings into agreement theory and observations. We have used the results from the previous sections to obtain SFR estimators that are free from these systematic effects,

$$\left. \begin{aligned} SFR(H\alpha)(M_{\odot} \text{yr}^{-1}) &= 1.1 \times 10^{-41} L_{H\alpha}(\text{erg s}^{-1}) \\ SFR([\text{OII}](M_{\odot} \text{yr}^{-1})) &= 8.4 \times 10^{-41} L_{\text{OII}}(\text{erg s}^{-1}) \\ SFR(\text{UV})(M_{\odot} \text{yr}^{-1}) &= 6.4 \times 10^{-28} L_{\nu}(\text{erg s}^{-1} \text{Hz}^{-1}) \end{aligned} \right\} (12)$$

where the SFR(H $\alpha$ ) is obtained from the reddening corrected H $\alpha$  luminosity while the expressions for the SFR(OII) and the SFR(UV) are for the observed fluxes.

These estimators, (the SFR(OII) and the SFR(UV) from equation 12) should be applied to samples where it is not possible to determine the extinction. If the objects have similar properties to our selected sample, then any systematic difference between the different estimators should be small.

We have applied this new set of calibrations to the SFR values given by different authors at different redshifts: Gallego et al. (1995) H $\alpha$  survey for the local Universe, Cowie et al. (1995) [OII] $\lambda 3727$  sample and Lilly et al. (1995) UV continuum one between redshifts of 0.2 and 1.5 and Connolly et al. (1997) between 0.5 and 2; and the UV points by Madau et al. (1996) and Steidel et al. (1999) at redshift higher than 2.5. We give in Table 3 the complete list of surveys of star formation at different redshifts that we have used plus their different tracers and computed SFR.

The results are plotted in Figure 9. We have also plotted the results obtained by Hughes et al. (1998) based on SCUBA observations of the Hubble Deep Field, those by Chapman et al. (2001) based on sub-millimeter observations of bright radio sources and those by Rowan-Robinson et al. (1997) based on observations at 60  $\mu\text{m}$  of the Hubble Deep Field. Clearly the mm/sub-mm results and our “unbiased” results agree within the errors. The “unbiased” history of star formation is characterized by a large increase of the SFR density from  $z \sim 0$  to  $z \sim 1$  (a factor of about 20) and a slow decay from  $z \sim 2$  to  $z \sim 5$ .

The final corrected values are similar to other published results (e.g. Somerville, Primack and Faber 2001). But the fact that our procedure removes systematic (or zero point) differences between the different estimators, implies that the shape of the curve, and therefore the slopes between  $z = 0$  and  $1$  and  $z = 1$  and  $4$  are now better determined.

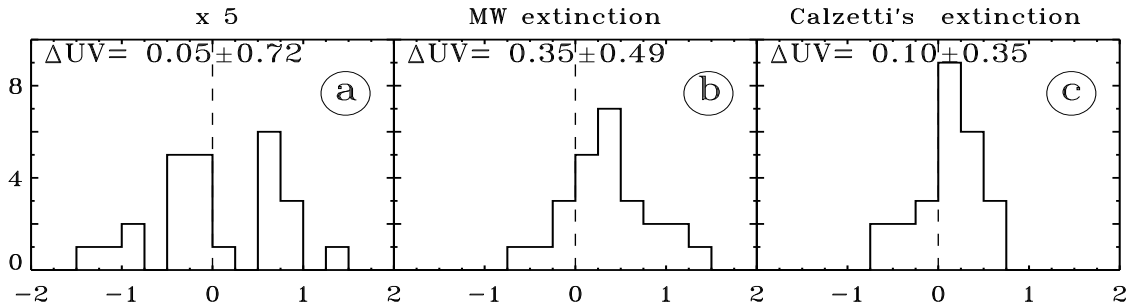


**Figure 8.** Histograms of the SFR given by the UV continuum normalized to the SFR(FIR). In the left panel we show the original data with the fixed correction given by Steidel et al. (1999). The central and right panels show the  $\Delta\text{UV}$  corrected for dust extinction computed including the underlying Balmer absorption (see Section 5.1) and photon escape. The median and standard deviation are given for each case. The total number of objects is 25.

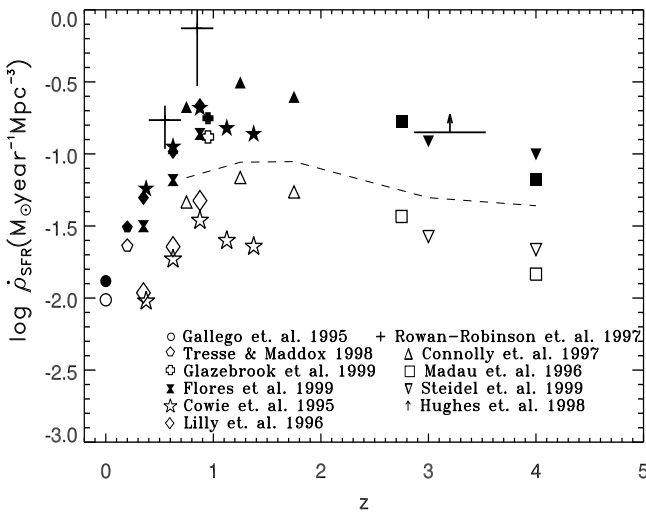


**Figure 9.** The SFR density as a function of redshift. The solid and open symbols represent values corrected and uncorrected for reddening respectively, except for the  $\text{H}\alpha$  values (the two lowest  $z$  points) which are all reddening corrected. The SFR in all cases are estimated using equations 2, 3, 4 and 5 for open symbols and equations 12 for the filled symbols. The open circle is the SFR based on  $\text{H}\alpha$  emission line corrected by extinction from Gallego et al. (1995) sample. The open stars are the SFR determined by  $[\text{OII}]\lambda 3727$  from the sample of Cowie et al. (1995) without any correction. The UV continuum samples are from Connolly et al. (1997) (triangles) Madau et al. (1996) (squares) and Steidel et al. (1999) (upside down triangles). The upward arrow is the lower limit given by Hughes et al. (1998) based on sub-mm observations of the Hubble Deep Field. The crosses at  $z = 0.55$  and  $0.85$  correspond to the SFR estimates by Rowan-Robinson et al. (1997). The dashed line is the lower limit given by Chapman et al. (2001).

## 7 THE HISTORY OF STAR FORMATION OF THE UNIVERSE

Let's now analyze with some detail the behaviour of the dust corrected curve of Figure 9.

Figure 10 shows the corrected curve together with some representative theoretical models; (the details of the differ-

ent sets of data are listed in table 3). Our basic assumption is that the main results from our sample of galaxies in the nearby universe are also applicable to samples of starforming galaxies at intermediate and high redshift.

An important result is that within observational errors, our calibrations succeed in bringing into reasonable agreement the FIR determinations with the optical/UV ones. A first implication of this agreement is that large dust extinction corrections are not favoured. It can be seen that while the general trend present in previous determinations of the star formation history is preserved, the rise from  $z = 0$  to  $z = 1$  is steeper than in most previous work. The procedure we have used minimizes any systematic differences between the different redshift ranges and implies that, provided the composition of the sample of objects at intermediate and high redshift is similar to that of our nearby sample, the shape of the curve would be preserved.

The general behaviour of the star formation history of the universe can be represented with a steep rise in the SFR rate from  $z = 0$  to  $z = 1$  with  $\text{SFR} \propto (1+z)^{4.5}$  and a decline from  $z = 1$  to  $z = 4$  where  $\text{SFR} \propto (1+z)^{-1.5}$  (see solid lines in Figure 10). The steep increase to  $z = 1$  is similar to the slope found by Glazebrook et al. (1999) using the  $\text{H}\alpha$  luminosities only.

We are confident that the procedure presented in this paper guarantees the removal of systematic differences between the star formation estimators when they are applied to samples qualitatively similar to ours. This in turn means that the general shape and in particular the slope from  $z = 0$  to  $z = 1$  and from  $z = 1$  to  $z = 4$  are well determined, although the exact value of the  $z = 0$  to  $z = 1$  slope is still very dependent on the exact value of the SFR in the nearby universe.

We also included in Figure 10 the results from some representative semi-analytical models of galaxy formation corresponding to the hierarchical cold dark matter scenario. The dotted lines correspond to Somerville et al. (2001)  $\tau\text{CDM}$  models with two different normalizations while the dashed line corresponds to model C from Baugh et al. (1998).

Whatever the local value of the SFR is, the comparison with these models of galaxy formation shows a general

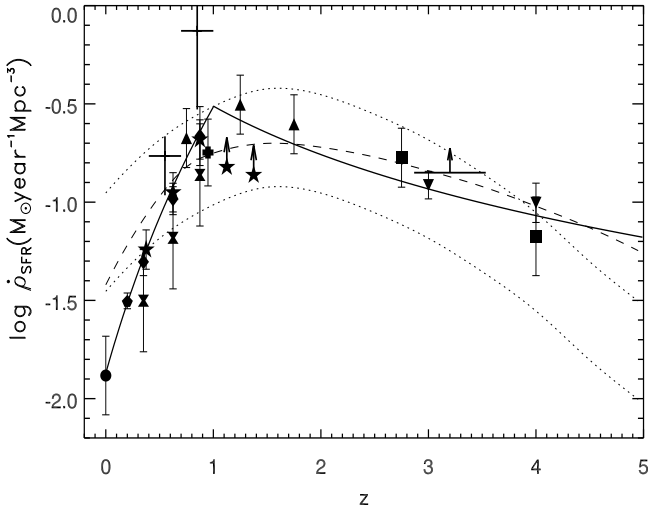


**Figure 10.** The unbiased SFR density as a function of redshift. The dotted lines represent the two normalizations in Somerville et al. (2001)  $\tau$ CDM models, and the dashed line is model C from Baugh et al. (1998). The solid lines represent  $\text{SFR} \propto (1+z)^{4.5}$  from  $z=0$  to  $z=1$  and  $\text{SFR} \propto (1+z)^{-1.5}$  for  $z>1$ .

agreement in the shape plus what we can call a local excess in the models, i.e. the models have a shallower slope between  $z=0$  to  $z=1$  than the data suggest or equivalently, that present semi-analytical models of galaxy formation seem unable to reproduce the sharp increase in the SFR from  $z=0$  to  $z=1$ .

## 8 CONCLUSIONS

One aspect that has generated many discussions regarding the SF history diagram in Cosmology, is the lack of confidence on the reddening corrections. This is compounded with the low level of agreement found until now between the optical/UV and FIR determinations of the SFR.

In the first part of this paper, we have investigated the possible systematic differences between SFR estimators by applying them to a sample of nearby star forming galaxies with good photometric data from the UV to the FIR.

We found that the main source of systematic differences among the SFR rate estimators is related to the presence of stellar Balmer absorption in the spectrum of emission line galaxies. The main effect of the Balmer absorptions is to produce an overestimate of the reddening when their effect is not included. We showed that taking into account the underlying Balmer absorptions effect in the estimates of reddening, removes most of the systematic differences between the SFR estimators in the optical/UV and FIR. Furthermore the scatter of the SFR estimations is considerably reduced by the application of the corrections. We also found that the escape of photons plays a minor role compared to that of the Balmer absorptions. These results give renewed confidence to the estimates of SFR for star forming galaxies in general and for samples similar to the one presented here in particular.

Thus, our central result is that the extinction correction including the effects of an underlying stel-

lar Balmer absorption brings into agreement all four SFR estimators, and that the photon escape correction seems to play a minor role.

In the second part of the paper we used the average results for our sample to construct a set of “unbiased” SFR estimators. These “unbiased” SFR estimators expressions include statistically the underlying Balmer absorption and photon escape corrections to the extinction estimates and bring the four SFR estimators studied here into the same system. We thus obtained consistent results between the SFR estimators in the optical/UV and FIR. The application of these “unbiased” SFR estimators to a compilation of surveys has produced a SFR history of the universe where all surveys results agree within the errors. Particularly important is the level of agreement achieved between the FIR/mm and optical/UV SFR results.

Our “new” and unbiased SFR history of the universe shows a steep rise in the SFR rate from  $z=0$  to  $z=1$  with  $\text{SFR} \propto (1+z)^{4.5}$  followed by a mild decline for  $z>2$  where  $\text{SFR} \propto (1+z)^{-1.5}$ . The steep increase to  $z=1$  seems in line with recent determinations of the SFR using only the  $\text{H}\alpha$  estimator. Most galaxy formation models tend to have a much flatter slope from  $z=0$  to  $z=1$ .

## 9 ACKNOWLEDGMENTS

We acknowledge fruitful conversations with Miguel Mas-Hesse, Daniela Calzetti, Piero Madau, Max Pettini, Divakara Mayya, Enrique Pérez, Rosa González-Delgado, David Hughes and Enrique Gaztañaga and useful suggestions from an anonymous referee. Daniel Rosa González gratefully acknowledges a research grant from the INAOE Astrophysics Department, a studentship from CONACYT, the Mexican Research Council, as part of ET research grant # 32186-E, and an EC Marie Curie studentship at the IoA Cambridge.

## REFERENCES

- Baugh, C. M., Cole, S., Frenk, C. S. and Lacey, C. G. : 1998, *ApJ* **498**, 504
- Calzetti, D., Kinney, A. L., and Storchi-Bergmann, T.: 1994, *ApJ* **429**, 582
- Calzetti, D.: 1999, *Astrophysics and Space Science* **266**, 243
- Chapman, S. C., Scott, D., Steidel, C. C., Borys, C., Halpern, M., Morris, S. L., Adelberger, K. L., Dickinson, M., Giavalisco, M., and Pettini, M.: 2000, *MNRAS* **319**, 318
- Chapman, S.C., Richards, E., Lewis, G., Wilson G., and Barger A.: 2001 *ApJL* **548**, L147
- Connolly, A. J., Szalay, A. S., Dickinson, M., Subbarao, M. U. and Brunner, R. J. : 1997, *ApJ* **486**, L11
- Cowie, L. L., Hu, E. M. and Songaila, A.: 1995, *Nat* **377**, 603
- De Vaucouleurs, G., De Vaucouleurs, A., Corwin JR., H., Buta, R. J., Paturel, G., and Fouque, P.: 1991, *Third Reference Catalogue of Bright Galaxies, version 3.9*
- Dickinson, M.: 1998, in *The Hubble Deep Field*, ed. M. Livio, S.M. Fall and P. Madau (Cambridge: Cambridge Univ. Press), 219
- Flores, H., Hammer, F., Thuan, T. X., Césarsky, C., Desert, F. X., Omont, A., Lilly, S. J., Eales, S., Crampton, D. and Le Fèvre, O.: 1999, *ApJ* **517**, 148
- Gallagher, J. S., Hunter, D. A., and Bushouse, H.: 1989, *AJ* **97**, 700

Redshift Range	SFR Tracer	$\log(\mathcal{L})$	$\log(\text{SFR})$ (Standard)	$\log(\text{SFR})$ (Unbiased)	Log Error	References
0.0-0.045	$\text{H}\alpha$	39.09	-2.01	-1.87	0.2	(Gallego et al. 1995)
0.1-0.3	$\text{H}\alpha$	39.47	-1.63	-1.50	0.04	(Tresse & Maddox 1998)
0.75-1.0	$\text{H}\alpha$	40.22	-0.75	-0.88	0.17	(Glazebrook et al. 1999)
0.25-0.50	FIR	41.85	-1.50	-1.50	0.26	(Flores et al. 1999)
0.50-0.75	FIR	42.17	-1.18	-1.18	0.26	(Flores et al. 1999)
0.75-1.00	FIR	42.49	-0.86	-0.86	0.26	(Flores et al. 1999)
0.25-0.50	OII	38.83	-2.02	-1.24	0.1	(Cowie et al. 1995)
0.50-0.75	OII	39.12	-1.73	-0.95	0.1	(Cowie et al. 1995)
0.75-1.00	OII	39.39	-1.46	-0.68	0.1	(Cowie et al. 1995)
1-1.25	OII	39.25	-1.60	-0.82	†	(Cowie et al. 1995)
1.25-1.50	OII	39.21	-1.64	-0.86	†	(Cowie et al. 1995)
0.25-0.50	UV	25.89	-1.96	-1.30	0.07	(Lilly et al. 1996)
0.50-0.75	UV	26.21	-1.64	-0.98	0.08	(Lilly et al. 1996)
0.75-1.00	UV	26.53	-1.32	-0.66	0.15	(Lilly et al. 1996)
0.4-0.7	FIR	42.64	-0.76	-0.76	(+0.1)(-0.2)	RR97
0.7-1.0	FIR	43.23	-0.13	-0.13	(+0.4)(-0.2)	RR97
0.5-1.0	UV	26.52	-1.33	-0.63	0.15	(Connolly et al. 1997)
1.0-1.5	UV	26.69	-1.16	-0.50	0.15	(Connolly et al. 1997)
1.5-2.0	UV	26.59	-1.26	-0.60	0.15	(Connolly et al. 1997)
2.0-4.0	FIR	42.80	-0.85	-0.85	†	(Hughes et al. 1998)
2.0-3.5	UV	26.42	-1.43	-0.77	0.15	(Madau et al. 1996)
3.5-4.5	UV	26.02	-1.83	-1.17	0.2	(Madau et al. 1996)
2.8-3.3	UV	26.28	-1.57	-0.91	0.07	(Steidel et al. 1999)
3.9-4.5	UV	26.19	-1.66	-1.00	0.1	(Steidel et al. 1999)

**Table 3.** SFR for surveys at different redshifts. The mean luminosity density ( $\mathcal{L}$ ) is given in units of  $\text{erg s}^{-1}\text{Mpc}^{-3}$  for the case of the  $\text{H}\alpha$  and OII emission lines and the FIR. The UV is given in  $\text{erg s}^{-1}\text{Hz}^{-1}\text{Mpc}^{-3}$ . The SFR referred to as standard are given by the expressions by Kennicutt (1998) and described in Section 3. The SFR referred to as unbiased are the ones obtained by using Equation 12. In both cases, the SFR are given in units of  $M_{\odot}\text{yr}^{-1}\text{Mpc}^{-3}$ .

- Gallego, J., Zamorano, J., Aragon-Salamanca, A., and Rego, M.: 1995, ApJL **455**, L1
- Gallego, J., Zamorano, J., Rego, M., Alonso, O., and Vitores, A. G.: 1996, A&AS **120**, 323
- Giavalisco M., Steidel C. C., Macchetto, F. D. : 1996, ApJ **470**, 189
- Glazebrook, K., Blake, C., Economou, F., Lilly, S. and Colless, M. : 1999, MNRAS **306**, 843
- González Delgado, R. M., Leitherer, C., and Heckman, T. M.: 1999, ApJS **125**, 489
- Heckman, T.M., Sembach, K.R., Meurer, G.R., Leitherer, C., Calzetti, D., Martin, C.L.:2001, astro-ph:0105012
- Howarth, I. D.: 1983, MNRAS **203**, 301
- Hughes, D. H., Serjeant, S., Dunlop, J., Rowan-Robinson, M., Blain, A., Mann, R. G., Ivison, R., Peacock, J., Efstathiou, A., Gear, W., Oliver, S., Lawrence, A., Longair, M., Goldschmidt, P., and Jenness, T.: 1998, Nature **394**, 241
- Kennicutt, R. C., J.: 1992, ApJ, 388, 310
- Kennicutt, R. C., J.: 1998, ARAA **36**, 189
- Kennicutt, R. C., J., Tamblyn, P., and Congdon, C. E.: 1994, ApJ **435**, 22
- Kinney, A. L., Bohlin, R. C., Calzetti, D., Panagia, N., and Wyse, R. F. G.: 1993, ApJS **86**, 5
- Koo D. C., Vogt N. P., Phillips A. C., Guzman R., Wu K. L., Faber S. M., Gronwall C., Forbes D. A., Illingworth G. D., Groth E. J., Davis M., Kron R. G., Szalay A. S.: 1996, ApJ **469**, 535
- Leitherer, C. and Heckman, T. M.: 1995, ApJS **96**, 9
- Lilly, S. J., Tresse, L., Hammer, F., Crampton, D., and Le Fevre, O.: 1995, ApJ **455**, 108
- Lilly, S. J., Le Fevre, O., Hammer, F. and Crampton, D. :1996, ApJL **460**, L1
- Lowenthal J. D., Koo D. C., Guzman R., Gallego J., Phillips A., Faber S. M., Vogt N. P., Illingworth G. D., Gronwall, C.: 1997, ApJ **481**, 673
- Madau, P. , Ferguson, H. C. , Dickinson, M. E. , Giavalisco, M. , Steidel, C. C. and Fruchter, A.: 1996 MNRAS **283**, 1388
- Madau, P., Pozzetti, L., and Dickinson, M.: 1998, ApJ **498**, 106
- Mas-Hesse, J. M. and Kunth, D.: 1991, ApJ **88**, 399
- Mayya, Y. D.: 1995, AJ **109**, 2503
- McQuade, K., Calzetti, D., and Kinney, A. L.: 1995, ApJS **97**, 331
- Meier, D. L. and Terlevich, R.: 1981, ApJL **246**, L109
- Meurer, G. R., Heckman, T. M., Lehnert, M. D., Leitherer, C. and Lowenthal, J.,:1997 AJ **114**, 54
- Meurer, G. R., Heckman, T. M., and Calzetti, D.: 1999, ApJ **521**, 64
- Moshir, M., Kopan, G., Conrow, T., McCallon, H., Hacking, P., and et al. : 1990, *Infrared Astronomical Satellite Catalogs*
- Olofsson, K.: 1995, AAPS **111**, 57
- Osterbrock, D. E.: 1989, *Astrophysics of Gaseous Nebulae and Active Galactic Nuclei*, University Science Books. Mill Valley, CA
- Rowan-Robinson, M. and Efstathiou, A.:1993, MNRAS **263**, 675
- Rowan-Robinson, M., Mann, R. G., Oliver, S. J., Efstathiou, A. and et al. :1997, MNRAS **289**, 490
- Seaton, M. J.: 1979, MNRAS **187**, 73P
- Somerville, R. S., Primack, J. R., Faber, S. M. : 2001, MNRAS **320**, 504
- Steidel, C. C., Adelberger, K. L., Giavalisco, M., Dickinson, M., and Pettini, M.: 1999, ApJ **519**, 1
- Steidel, C. C., Pettini, M. and Adelberger, K. L. : 2001, ApJ **546**, 665
- Storchi-Bergmann, T., Kinney, A. L., and Challis, P.: 1995, ApJS **98**, 103
- Tenorio-Tagle, G., Silich, S. A., Kunth, D., Terlevich, E. and Ter-

- levich, R.: 1999, MNRAS **309**, 332  
 Terlevich, E., Diaz, A. I., Terlevich, R., and Vargas, M. L. G.: 1993, MNRAS **260**, 3  
 Terlevich, R., Melnick, J., Masegosa, J., Moles, M., and Copetti, M. V. F.: 1991, A&AS **91**, 285  
 Tresse, L. and Maddox, S. J.: 1998, ApJ **495**, 691

## APPENDIX A: DUST EXTINCTION CORRECTIONS TO THE OBSERVED FLUXES

Two different extinction curves are used: the Milky Way extinction law (MW) given by Seaton (1979) and Howarth (1983) and the Large Magellanic Cloud one (LMC) given by Howarth (1983). The main parameters of both laws are given in Table A1.

### A1 Dust Extinction Corrections to the Continuum Fluxes

Calzetti and collaborators developed an empirical method to estimate the UV extinction (Calzetti, Kinney and Storchi-Bergmann, 1994). They found that the power-law index  $\beta$  in the ultraviolet defined as  $F_\lambda \propto \lambda^\beta$  is well correlated with the difference in optical depth between H $\alpha$  and H $\beta$  defined as  $\tau_B^l = \ln \left( \frac{F(H\alpha)/F(H\beta)}{2.86} \right)$  where  $F(H\alpha)$  and  $F(H\beta)$  are the intensities of the H $\alpha$  and H $\beta$  emission lines respectively. This correlation, which is linear and independent of the adopted extinction law is given by,

$$\beta = (1.76 \pm 0.25)\tau_B^l - (1.71 \pm 0.12) \quad (A1)$$

The parameter  $\beta$  is obtained by fitting the power law to the IUE ultraviolet spectra. Calzetti et al. (1994) and Meurer, Heckman and Calzetti (1999) values of  $\beta$  are presented in Table 2 as well as our estimate for CAM0840, CAM1543, TOL1247, ESO572 and MRK309.

The effect of reddening using different dust spatial distributions can be estimated from Equation A1 by comparing ultraviolet with optical spectra. Calzetti et al. (1994) estimate the optical depth  $\tau_\lambda$  by solving the transfer equation for five different geometries, uniform or clumpy dust screen, uniform or clumpy scattering slab and internal dust. The uniform dust screen constitutes the easiest case where the optical depth is related to the visual extinction by

$$\tau_\lambda = 0.921k(\lambda)E(B - V)$$

where  $E(B-V)$  is the colour excess and  $k(\lambda)$  is the extinction law. For the other geometries, apart from the assumed extinction law, the optical depth is a function of dust parameters such as the albedo, the phase parameter or the number of clumps. After comparing synthetic extinction corrected spectra with observations of emission line galaxies Calzetti et al. (1994) conclude that none of the adopted geometries combined with the *standard* MW and LMC extinction laws could explain the observed tight relation between  $\tau_B^l$  and  $\beta$  and proposed an empirical extinction law obtained from IUE spectra of a sample of nearby starburst galaxies.

Calzetti et al. (1994) created 6 different templates averaging galaxies with the same amount of dust (judging by their Balmer decrements). The template with  $\tau_B^l = 0.05$  is taken as the reference one (free of dust). An optical depth,  $\tau_n(\lambda)$ , is calculated for each template by comparing the observed fluxes,  $F_n(\lambda)$  and  $F_1(\lambda)$ ,

$$\tau_n(\lambda) = -\ln \frac{F_n(\lambda)}{F_1(\lambda)} \quad (A2)$$

where the subindex 1 corresponds to the dusty free template and the subindex n corresponds to the n template. For each template a rescaled optical depth can be defined

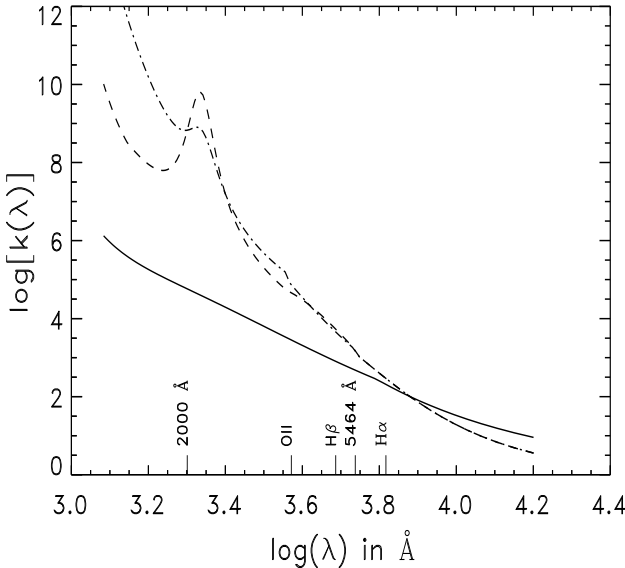


**Figure A1.** Adopted extinction curves. The solid line is the empirical relation given by Calzetti (1999). The dashed line is the curve for the MW (Seaton (1979) and Howarth (1983)) and the dot-dashed line is the curve for the LMC (Howarth 1983).

$$Q_n(\lambda) = \frac{\tau_n(\lambda)}{\tau_{Bn}^l - \tau_{B1}^l(\lambda)} \quad (A3)$$

Averaging this quantity, Calzetti et al. (1994) found an extinction curve,  $Q(\lambda)$  which can be transformed to  $k(\lambda)$  (e.g. Seaton, 1979) by,

$$Q(\lambda) = \frac{k(\lambda)}{k(H\beta) - k(H\alpha)} \quad (A4)$$

where the difference  $k(H\beta) - k(H\alpha)$  is given by the Seaton (1979) extinction curve. The observed ultraviolet flux is related to the emitted one by,

$$F_{obs}(\lambda) = F_o(\lambda)10^{-0.4Av k(\lambda)/R} \quad (A5)$$

where  $k(\lambda)$  is given by (Calzetti 1999)

$$k(\lambda) = -2.156 + 1.509/\lambda - 0.198/\lambda^2 + 0.011/\lambda^3 \quad (A6)$$

valid for the range  $0.12 \mu\text{m} < \lambda < 0.63 \mu\text{m}$ .

The obtained extinction curve can be considered as an average of the different dust distributions described by Calzetti et al. (1994).

In order to correct the ultraviolet flux using this procedure it is necessary to estimate  $Av$  from the observed  $H\alpha/H\beta$  ratios and then apply Equation A6 to the observed ultraviolet fluxes. Physically this correction is understood assuming that the ionized gas is more affected by extinction than the stars which are producing the observed UV flux (Calzetti et al. 1994).

No corrections were applied to the IR data.

The different extinction curves are plotted in Figure A1.

## A2 Dust extinction corrections to the Emission Line Fluxes

Extinction affects the emission lines in different degrees depending on wavelength. Corrections are usually obtained from the observed ratio of Balmer lines, the intrinsic ratio, and an adopted interstellar extinction curve.

The ratio between the intensity of a given line  $F(\lambda)$  and the intensity of  $H\beta$ ,  $F(H\beta)$  can be expressed by:

$$\frac{F(\lambda)}{F(H\beta)} = \frac{F_o(\lambda)}{F_o(H\beta)} 10^{-0.4Av[k(\lambda) - k(H\beta)]/R} \quad (A7)$$

where the difference  $k(\lambda) - k(H\beta)$  is tabulated for different extinction laws (Table A1). The total visual extinction  $Av$ , depends on the observed object (see Table 2). The subindex  $o$  indicates the unreddened values. We use as reference the theoretical ratio for Case B recombination  $F_o(H\alpha)/F_o(H\beta) = 2.86$  and  $F_o(H\gamma)/F_o(H\beta) = 0.47$  (Osterbrock 1989). The observed flux ratios can be expressed as a function of the theoretical ratios and the visual extinction,

$$\begin{aligned} \log \frac{F(H\alpha)}{F(H\beta)} &= \log 2.86 - 0.4[k(H\alpha) - k(H\beta)]Av/R \\ \log \frac{F(H\gamma)}{F(H\beta)} &= \log 0.47 - 0.4[k(H\gamma) - k(H\beta)]Av/R \end{aligned} \quad (A8)$$

This Equation was used to analyze the presence of an underlying stellar population in Section 5.1.

This paper has been produced using the Royal Astronomical Society/Blackwell Science L<sup>A</sup>T<sub>E</sub>X style file.

	$k(\text{H}\alpha) - k(\text{H}\beta)$	$k(\text{H}\gamma) - k(\text{H}\beta)$	$R = k(5464 \text{ \AA})$	$k([\text{OII}]\lambda 3727)$	$k(1700 \text{ \AA})$
MW	- 1.25	0.45	3.2	4.67	7.80
LMC	- 1.18	0.48	3.2	4.86	9.54
Calzetti	- 0.58	0.23	2.7	3.46	5.10

**Table A1.** Adopted values for the extinction curves.